Performance of Unslotted ALOHA with Capture and Multiple Collisions in LoRaWAN

Martin Heusse, Christelle Caillouet, Andrzej Duda

This article has been accepted for publication in IEEE Internet of Things Journal. This is the author's version which has not been fully edited and content may change prior to final publication. Citation information: DOI 10.1109/JIOT.2023.3280393

Performance of Unslotted ALOHA with Capture and Multiple Collisions in LoRaWAN

Martin Heusse, Christelle Caillouet, and Andrzej Duda *Member, IEEE*

***Abstract*—This paper explores the capacity limits and the tradeoff between the antagonistic means of enabling reliable data delivery in a loaded LoRaWAN cell. In fact, channel attenuation and variability call for robust transmission settings but the associated load increase causes more collisions between frames. In addition to the physical layer parameters of the LoRa modulation, this paper considers the benefits and tuning of inter-packet Error Correction Codes (ECC), which also trades transmission redundancy for reliability. We thus start by proposing a refined Packet Delivery Ratio (PDR) model that improves the ones found in the literature in that, first, it takes into account the dependency between overcoming ambient noise and dominating colliding frames, and second, it considers the sum of interference powers when multiple colliding frames are present, even if the interference preexists. Moreover, the model extends to the case of a gateway with receiver diversity. In a second step, the model allows to set out the level of redundancy at which ECC is the most effective without hindering capacity: a coding rate of one third. When this is fixed, it allows to define the transmission parameters allocation within a cell and thus the size of the cell. We finally develop an ad-hoc Python discrete-event simulator, freely accessible, to complement the model for assessing the effect of inter-SF and near-far interference and to show the benefits of power control in this respect.**

***Index Terms*—LoRa, LoRaWAN, unslotted ALOHA, Packet Delivery Ratio, Capture effect, Network capacity, Coverage**

I. Introduction

LoRa®(Long Range) is a recent LPWAN (Low Power Wide Area Networks) technology that supports low-power long range communications oriented towards IoT (Internet of Things) applications [1]. It uses a specific radio layer based on the CHIRP (Compressed High Intensity Radar Pulse) Spread Spectrum (CSS) modulation that gives access to a number of data rates providing various levels of transmission robustness. LoRaWAN® [2] specifies a communication protocol over the physical layer and the network architecture. We focus on Class A (for All end-devices [2]) uplink communications in which the devices access the channel exclusively using the unslotted ALOHA protocol [3], [4]: a device wakes up and can send a packet at any instant on a chosen radio channel, provided its duty cycle follows the frequency band regulations (typically 1 % in the 868 MHz band under EU regulations). One or several gateways may receive the packet and forward it to Network and Application Servers.

Martin Heusse and Andrzej Duda are with the Univ. Grenoble Alpes, CNRS, Grenoble INP, LIG, 38000 Grenoble, France.
martin.heusse@univ-grenoble-alpes.fr, andrzej.duda@univ-grenoble-alpes.fr

Christelle Caillouet is with Université Côte d'Azur, I3S, CNRS, Inria, 06903 Sophia Antipolis, France.
christelle.caillouet@univ-cotedazur.fr

As sending downlink packets to a large number of devices may overload the channel and would make the gateways exceed the duty cycle limitation, network operators discourage their use and most end-devices send the *Unconfirmed* type of packets.[1] So, unlike most implementations of ALOHA (e.g., the random access channel of cellular networks), LoRaWAN transmissions are not acknowledged and devices are not aware of packet losses. They do not immediately re-schedule lost packets and they just send data at the instants defined by the application within the limits of the duty cycle. In such a setup, the crucial measure of LoRaWAN performance is Packet Delivery Ratio (*PDR*) and utilization $U = PDR \times v$, where v is the channel load [6].

Achieving high network utilization is important for network operators as there is a tradeoff between the coverage range of a LoRaWAN cell and the load generated by end-devices: it is less costly to deploy the gateways far apart from each other, but then, nodes have to use a more robust modulation resulting in longer transmission times, which in turn increases channel load v and collisions, thus reducing the *PDR*. As in most cellular systems, there must be more gateways in the areas with a higher density of nodes, and an underloaded cell is a waste of ressources (except for ensuring coverage in low density areas). Thus, we need an accurate model of LoRaWAN cell capacity to achieve the best tradeoff and optimize utilization.

This paper addresses the performance modeling of LoRaWAN cell capacity, crucial to the study of wide deployments of such networks in dense environments that can serve thousands of connected IoT objects. We propose a PDR model validated by simulations that expresses jointly the impact of channel variability and collision-related losses on cell performance. As the unslotted ALOHA access method and the absence of packet acknowledgments result typically in low levels of PDR, even below 50%, there is a need for transmission redundancy to achieve reliable data delivery. Our results, based on the model for tuning inter-packet Error Correction Codes (ECC), show that for a wide range of the distance to the gateway, a redundancy level of 3 is the best tradeoff, a characteristic value for unslotted ALOHA. We also show that this level of redundancy allows to operate at the maximal channel utilization working point. Moreover, we show that more redundancy is counter productive at a short distance but allows to increase coverage range at the cost of traffic capacity.

[1]The Things Networks asks that downlink or *Confirmed* messages be avoided as much as possible [5]. Orange Liveobjects charges downlink transmissions on a per-packet basis.

Several authors proposed models of the LoRaWAN operation to evaluate scalability and capacity of a cell in terms of *PDR* for a given number of devices around a gateway and depending on the distance to the gateway [7], [8], [9], [10], [11], [12]. Unlike previous work, our model is more precise because it takes into account the dependency between overcoming ambient noise and dominating colliding packets. The first published LoRaWAN models [7], [8] assumed the independence of these two events and a number of the ensuing papers adopted the same assumption. Our model also considers the sum of interference powers when multiple colliding packets are present, even if the interference preexists, in keeping with the capabilities of the current SX1302 chips to lock on a signal even if a reception is ongoing on the same channel and SF. Only few studies considered the benefits of redundancy for LoRaWAN [13] while our model allows us to analyze the required redundancy for the best channel utilization.

Before studying a cell with randomly placed nodes using different SFs, we focus on the problem of contention involving all devices that use the same channel and the same value of the spreading factor (*SF*), when they are all placed at roughly the same distance to the gateway. We assume, unless stated otherwise, that transmissions using different spreading factors are quasi-orthogonal [14], [11]: except for specific near-far conditions, the gateway can receive simultaneous transmissions using different values of *SF*. We also neglect the impact of the limited number of demodulators in the gateway [15], which is less limiting for the 16 reception paths of the SX1302 vs. 8 for older chips. We derive a new model of the unslotted ALOHA performance in LoRaWAN that takes into account the fact that channel conditions, i.e., the multipath random gain, are the same both for deciding if the frame can be successfully demodulated and for dominating the sum of co-SF interference [12]. We also consider receiver diversity, a classic measure to mitigate multipath fading.

Besides the model itself, the contributions of this paper are the following:

- we show that the capability of current gateways to lock on a new signal, even if it collides with earlier frames, has very significant benefits in terms of network capacity;
- aligning the capacity to the traffic demand and thus approaching maximal channel utilization requires to be able to deal with a *PDR* of less than 50% and often around 33%;
- consequently, reliable data delivery imposes to use an inter-packet ECC with the right parameters to maximize the goodput, i.e., the volume of application data delivered per time unit;
- we derive the best level of redundancy, corresponding to *three* packet transmissions per successful reception, a characteristic value for unslotted ALOHA, unless the deployment focuses only on increasing communication range;
- we show that receiver diversity results in a significant capacity improvement at all distances, including near the gateway where transmissions at any SF succeed;
- we provide discrete-event simulations showing that power control, applied solely to the nodes that are close to the gateway and that use SF7, is effectual to reduce near-far unfairness as well as inter-SF interference.

The paper is structured as follows. Section II presents related work on the performance modeling and on the capacity evaluation of LPWAN. Section III recalls the basic principles of LoRaWAN and introduces the *PDR* model in case of capture and multiple collisions. In Section IV, we validate the model and present the comparisons with simulations for the cases with and without receiver diversity. Section V discusses the implications of the proposed model on using the channel at high load and achieving good transmission reliability despite *PDR* of the order of 30-50%. Section VI optimizes the *SF* allocation for various node densities, compares the results with previous work, and analyzes power control in the *SF7* zone. Section VII concludes the paper.

II. Related Work

Modeling LoRaWAN performance needs to take into account several aspects. First, the baseline and most conservative model for LoRaWAN is the well-known ALOHA collision model [3], [16] in which any overlap between two transmissions causes both packets to be lost. In this case, the maximum channel utilization is $U \leq 1/(2e) \approx 18.4\,\%$. However, in reality in LoRaWAN, a small overlap between the end of a transmission and the start of the next frame preamble does not always prevent receiver locking on the second frame, whereas the physical layer robustness to noise and interference also allows successful reception of the first frame. Collisions due to ALOHA access are a major cause of packet loss, even if the CSS modulation makes transmissions somewhat robust to interference so they may survive overlapping transmissions leading to the well known *capture effect* [4], [17], [18], [19], [20].

Second, successful packet reception depends on strongly varying channel conditions (e.g., Rayleigh fading [21]) and ensuring a high *PDR* would require very conservative transmission parameter adjustments at the LoRaWAN MAC layer with the use of for instance, the Adaptive Data Rate (ADR) mechanism. The LoRa modulation robustness and adaptivity sets it apart from other LPWAN technologies like SigFox [22] or Mioty [23], [24] in which all transmissions use the same narrow-band physical layer parameters.

Finally, achieving a high level of reliable data delivery of the order of 99% for instance, based on inherently unreliable packet transmissions calls for a level of transmission redundancy in the form of inter-frame ECC or repetitions. Forward error correction compensates for the impossibility to use per-packet acknowledgments for retransmitting lost packets on demand, due to the scarcity of downlink transmission opportunities. Both SigFox and Mioty rely on redundancy: SigFox devices transmit each frame three times, and Mioty splits each frame in short sub-packets transmitted using frequency hopping and an ECC with the $\frac{1}{3}$ coding rate.

More than two decades ago, Birk and Keren [25] studied the benefits of replication to improve utilization of an ALOHA channel, regardless of capture or losses due to thermal noise. Their study is more general than the one explored in this paper,

but they reach the conclusion that replication is beneficial and that the number of replications needs to be carefully chosen. Even though the pure ALOHA model is a simplification of LoRaWAN, it allows to obtain a baseline capacity estimation for LoRaWAN [10].

In contrast to previous work [7], [8], [9], [10], [11], [12], the model presented in this paper is more precise because we assume that the random channel gain is the same when it comes to deciding if the receiver can overcome thermal noise and if the considered frame dominates colliding frames. Therefore, unlike other LoRaWAN models, the premise of our model is that the two associated probabilities are dependent, which, combined with considering the sum of interference powers, constitutes the contribution of this paper with regard to modeling.

The independence assumption is an implicit simplification in the first published LoRaWAN models [7], [8] and a number of the ensuing papers adopted the same assumption. Some of this research assessed the impact of imperfect orthogonality between the signal at different *SF*s [9], [11], the benefits of antenna diversity [26], and Successive Interference Cancellation (SIC) [27]. The study by Sant'Ana et al. of the benefits of replication and coding for LoRaWAN [13] is the most related to the present paper. However, our model is more precise, we compare its results with simulations, and we assess the required redundancy for the best channel utilization regardless of the error correction scheme specifics. Moreover, we do not consider that only collisions matter as for instance in the study by Song et al. [28].

In this paper, we model the impact of collisions by means of a "co-channel rejection matrix" in which each element represents the power margin required for a reception to survive interference depending on the SF of both transmissions. This model is simple but Magrin et al. [29] showed that it leads to very similar results compared to more fine-grained collision modeling, e.g., when the probability of bit errors is computed taking into account the various SINR levels experienced during the reception of a frame.

While there are several indications that redundant transmissions improves the PDR for ALOHA networks [25] or LoRaWAN [21], this paper introduces a precise LoRaWAN model that takes into account the impact of both channel variability and collision related losses on cell performance. As a result, the model allows us to assess the level of redundancy that works the best, in conjunction with the optimal transmission parameter settings.

Recent interest in Machine-to-Machine (M2M) type communications within 5G cellular networks spawned research on ALOHA used along with Non-Orthogonal Multiple Access (NOMA) able to resolve collisions via the use of SIC at the receiver [30]. The advantage of ALOHA-NOMA is the increased utilization: for two contending devices, the maximum utilization goes up to $42\,\%$. We do not consider SIC in this paper, and neither the benefits of coherent combination of signals received on multiple antennas [31]. We also do not consider the demodulation of several LoRa signals in parallel by means of tracking the multiple peaks appearing in the FFT when frames collide [32], [33]. All these mechanisms have the potential to improve the scalability of LoRaWAN in terms of traffic intensity, with respect to the results presented in this paper.

Table I
LoRa physical layer parameters for 125 kHz bandwidth.

SF	DR*j*	Data rate [b/s]	PL_{max} [B]	Airtime τ_j [ms]	*SNR* limit q_j [dB]
7	DR5:	5469	230	102.7	-7.5
8	DR4:	3125	230	184.8	-10
9	DR3:	1758	123	328.7	-12.5
10	DR2:	977	59	616.5	-15
11	DR1:	537	59	1315	-17.5
12	DR0:	293	59	2466	-20

III. PDR Model with Capture and Multiple Collisions

In this section, we present the model for *PDR* in a LoRaWAN cell.

A. LoRa Basics

The LoRa physical layer depends on the following parameters [34]:

- **Spreading Factor (*SF*)** characterizes the number of bits carried by a CHIRP: *SF* bits map to one of the 2^{SF} possible frequency shifts. *SF* varies between 7 and 12: *SF12* gives best sensitivity and range at the cost of the lowest data rate and worst energy consumption. Increasing *SF* by 1 roughly doubles the transmission duration and, hence, energy consumption.
- **Coding Rate (*CR*)** of intra-frame Forward Error Correction (FEC) that improves the packet error rate in presence of noise and interference. A lower coding rate results in better robustness, but increases the transmission time and, hence, energy consumption. The possible values are: 4/5, 4/6, 4/7, and 4/8.
- **Transmission Power** (P_{t}): several values of P_{t} can be used in the EU 863-870 MHz band: 2 dBm, 4 dBm, 6 dBm, 8 dBm, 12 dBm, and 14 dBm.
- **Data rate (DR*j*)** depends on the chosen channel bandwidth, spreading factor *SF*, and coding rate *CR*: a higher bit rate results from lower *SF*, larger bandwidth, and *CR* of 4/5, at the cost of lower sensitivity and range. The bit rates range from 293 b/s to 11 kb/s: 293 b/s corresponds to *SF12* for 125 kHz bandwidth, whereas 11 kb/s results from *SF7* and 250 kHz bandwidth. Table I presents the main performance parameters: *SF*, data rate DR*j*, the maximum payload length (PL_{max}), the corresponding transmission airtime [35], and the *SNR* limit for demodulation [36].

Devices choose different values of *SF* depending on the distance to the gateway so that the *SF* boundaries in a cell form a set of annuli around the gateway.

B. Assumptions

We start by assuming that all devices using the same *SF* (transmission duration of τ_j and data rate DR*j*) are at the same

distance, and they contend for the same channel. This strong assumption is validated through simulations (see Section VI-B) in which our model reflects the degree of PDR variation within each SF zone and closely matches the results obtained by simulations except in the SF7 zone, in which the prediction is accurate only for the nodes at the zone edge, where it matters. Devices may adjust the value of *SF* using the ADR mechanism based on the experienced channel conditions in successful transmissions, so that the devices using the same *SF* effectively face similar average channel gains. Although devices may wake up at constant intervals, the superposition of traffic from a large number m_j of devices using DR*j* forms a homogeneous Poisson process with intensity λ_j. $v_j = \lambda_j \tau_j$ represents the offered traffic at data rate DR*j*. v_j is the dimensionless ratio between the offered load and the raw channel capacity, generally expressed in Erlang. Table II summarizes the notation.

We consider that the packet generation intensity by an individual node is $\lambda_t = \frac{\lambda_j}{m_j}$ (regardless of its assigned DR), which corresponds to the maximal duty cycle at DR*0* (*SF12*) using 59 B packets, the maximum size at this data rate.

The granularity of the duty cycle constraint is the frequency band: LoRa devices have to limit their occupation of each frequency band to 1% of time, with 3 to 5 frequency channels in each band. In Europe, for instance, there are 3 channels in band h1.5 and 5 in h1.4, so if we assume 3 channels, devices can use each of them at 0.33% duty cycle. The airtime of maximum size packets at DR*0* corresponds to $\tau_0 = 2.466\,\mathrm{s}$, so they can be sent every 739.8 s on the same channel (or every 246.6 s on different channels) to achieve 0.33% duty cycle ($\frac{1}{300}$) per channel. Thus, $\lambda_t = \frac{1}{739.8\,s}$.

We consider that transmissions using different spreading factors are quasi-orthogonal so that inter-SF interference is negligible [14], [11], [12]. We also assume that the wireless channel is subject to Rayleigh fading [21], [37].

We leave aside lognormal shadowing. Most LoRaWAN models neglect its effect and sometimes argue that there is none on average. Actually, shadowing increases the apparent node density [28], so that the below results are in fact conservative: with shadowing, the nodes appear on average closer than they actually are.

C. Postulates of the Capture Model for LoRaWAN

The design of the LoRa gateways, based for instance on the SX1302 chip or beyond [38], allows demodulation of multiple LoRa packets in parallel (16 packets with the SX1302) on a number of frequency channels (typically, 8 to 10). The data sheet describes how the preamble detection engine constantly scans for frames with any SF, so that "*the SX1302 can detect at any time, any packet in a combination of 8 different spreading factors (SF5 to SF12) and 10 channels…*".[2] When the preamble search engine finds a preamble, it delegates packet reception to one of 16 LoRa demodulators (for the SX1302 chip). Notably, preamble detection and frame acquisition is still possible even if a reception is already ongoing on the same frequency channel and SF (except for the case of overlapping preambles). Without independent preamble detection circuitry, the presence of an earlier preamble most often prevents the chip from locking on a subsequent stronger frame, as observed by Rahmadhani and Kuipers [39]. Our model thus differs from previous work that assumed the precedence of pre-existing frames [20], which does not reflect the operation of current gateways.[3]

To the best of our knowledge, there is no study of the conditions for locking on the preamble when two frames collide during the preambles, for the chips with a preamble search engine, but the observations by Rahmadhani and Kuipers offer a good starting point: in the case in which one frame is stronger than the other one (by for instance 6 dB [39]), the stronger frame is received with high likelihood if it arrives earlier or within the first four symbols of the weaker frame preamble. Otherwise, if the stronger frame is late but its preamble interferes with the LoRa PHY header Cyclic Redundancy Check (CRC) of the weaker frame, then the receiver switches to the new signal.

The observation by Rahmadhani and Kuipers gives us a baseline for preamble locking: in the worst case, with a preamble search engine of new chips that behaves like the older transceivers, the stronger frame would be lost only if it came after the first four symbols of the weak frame preamble and before its PHY header CRC. It means that only a small fraction of collisions leads to missing the new stronger preamble. Thus, we assume below the most favorable case—we do not distinguish the preamble from the rest of the transmission. A more conservative assumption would be to consider that an additional small fraction of collided frames would be lost.

Table II
NOTATION

Frame duration at data rate DR*j* and *SFj*	τ_j
Aggregate packet generation intensity at DR*j*	λ_j
Per node packet generation intensity	λ_t
Number of nodes that use DR*j*	m_j
Offered traffic (in Erlang) at DR*j* and *SFj* $\lambda_j \tau_j =$	v_j
Channel utilization *PDR* $\times v_j =$	U
Poisson process probability of witnessing n events	$P_n(v_j)$
Average channel gain at distance d	$g(d)$
SNR threshold for *DRj* and *SFj*	q_j
Random gain threshold for exceeding q_j	g_j
Power margin for successful capture (typically, 1 dB)	ξ
Transmission power	P_t
Inter-packet Error Correcting Code (ECC) Coding rate	C
In-band noise power	$\mathcal{N}$
Probability of successful reception, no collision [7]	H
Prob. of dominating interfering frames [27], [13]	Q_1
Number of other colliding frames	n
PDR of unslotted ALOHA, without diversity	$\boldsymbol{P}_{\mathrm{A}}$
PDR of unslotted ALOHA, with diversity	$\boldsymbol{P}_{\mathrm{A+D}}$
PDR in LoRaWAN, free channel condition [20]	$\boldsymbol{P}_{\mathrm{S}}$
PDR with capture (this contribution)	$\boldsymbol{P}_{\mathrm{C}}$
PDR with capture, with diversity (this contribution)	$\boldsymbol{P}_{\mathrm{C+D}}$
Goodput normalized by the channel capacity	G

[2]Only SF7 to SF12 are considered in LoRaWAN.

[3]The authors would like to thank B. Ning of Semtech for clarifying the chip behavior.

This article has been accepted for publication in IEEE Internet of Things Journal. This is the author's version which has not been fully edited and content may change prior to final publication. Citation information: DOI 10.1109/JIOT.2023.3280393

Consequently, we propose to model concurrent LoRa packet reception based on the following postulates:

- The timing of colliding frames does not significantly influence reception, as opposed to the situation in which an earlier preamble prevents locking on a subsequent frame.
- Packet reception is successful against thermal noise as long as the packet power exceeds the SNR threshold q_j for its *SF*.
- Packet reception succeeds against interference of other colliding frames if power margin ξ against co-SF interference is met all along the packet reception.
- We do not distinguish the case of a collision occurring during the preamble: only the strongest frame will be received in our model, whereas in reality, there is a possibility that it could be jammed by an earlier and weaker preamble.
- We consider that the likelihood of overcoming thermal noise (with probability H [7]) and interference (with probability Q_1 [7], [27], [13]) are not independent, in contrast with the common assumption of their independence adopted in most previous work [7], [8], [9], [11], [26], [27], [13] nor that losses are only due to collisions [28]

D. Modeling Successful Frame Capture in LoRaWAN

We decompose successful frame reception into several cases depending on the number n of colliding frames:

Case 1: $n = 0$: no interfering frame during a transmission,
Case 2: $n = 1$ colliding frame,
Case 3: $n = 2$ colliding frames,
Case 4: $n > 2$: more than 2 colliding frames.

We derive the successful frame reception for each case to finally obtain the expression for *PDR*.

Case 1: PDR for a Collision-free Transmission ($\mathbf{n = 0}$). The probability of receiving a frame when it is not subject to a collision is the following:

$$p_0 = H = e^{-g_j} \tag{1}$$

as the fast fading gain follows the $\exp(1)$ distribution. The threshold fast fading gain g_j is the value for which the reception power allows to reach q_j at distance d:

$$g_j = \frac{\mathcal{N}\, q_j}{P_{\mathrm{t}}\, g(d)}. \tag{2}$$

Case 2: PDR for $\mathbf{n = 1}$ Colliding Frame. The probability of successful reception of a frame of interest transmitted against another overlapping transmission is the probability that it dominates both the thermal noise and the interfering frame by factor ξ. This probability is the special case for $n = 1$ of the probability of successful reception of a frame of interest transmitted against n other colliding transmissions $p_\Sigma(n)$ given below (Eq. 8 in section III-D1) and derived in Appendix A.

$$p_1 = p_\Sigma(1) \tag{3}$$

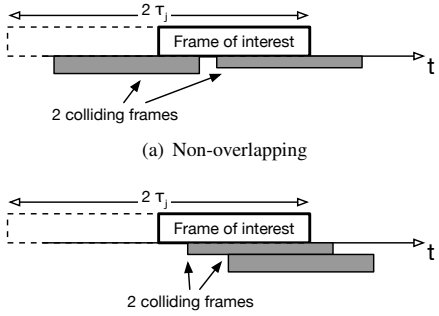

(a) Non-overlapping

(b) Overlapping

Figure 1. Collision with two other frames: overlapping and non-overlapping scenarios

Case 3: PDR for $\mathbf{n = 2}$ Colliding Frames. In presence of $n = 2$ other frames, we need to distinguish between two temporal positions of the interfering frames (see Figure 1):

i) with probability P_{NO} (derived below in Eq. 7), the colliding frames do not overlap, as in Figure 1(a);
ii) the colliding frames overlap as in Figure 1(b).

In the latter configuration, the frame of interest needs to dominate the *sum of interference powers* by factor ξ with probability $p_\Sigma(2)$. In the former, the interfering frames do not overlap each other and the impact of interference is reduced, but the frame of interest still has to prevail against the interference all along the reception by dominating *the maximum power* between the two interfering frames, with probability $p_{\max}(2)$, derived below (Eq. 9 in section III-D2).

$$p_2 = P_{\mathrm{NO}}\, p_{\max}(2) + (1 - P_{\mathrm{NO}})\, p_\Sigma(2) \tag{4}$$

Case 4: PDR for $\mathbf{n > 2}$ Colliding Frames. In this case, for tractability, we consider that $n > 2$ interfering frames always overlap so we use the expression for $p_\Sigma(n)$. This approximation leads to an underestimation of the reception success probability but it has little impact as, for the channel load of 0.75 Erlang, more than 80% of the frames encounter two or less colliding frames and otherwise, only few frames survive interference against three frames, as one can expect. Our comparison with simulations in Section VI shows the good accuracy of this approximation.

$$p_n \simeq p_\Sigma(n) \tag{5}$$

Final Expression for PDR. Given that the four considered cases are mutually exclusive and exhaustive, the *PDR* is simply the sum of all probabilities to succeed in face of 0, 1, 2, or more colliding frames weighted by the probabilities $P_n(v_j)$ of having $n = 0, 1, 2$, or more other colliding frames. As we assume a Poisson frame generation process, the probability of facing n colliding frames is $P_n(v_j) = \frac{(2v_j)^n}{n!} e^{-2v_j}$, and we

obtain the final expression for *PDR* as:

$$\begin{aligned}\boldsymbol{P}_{\mathrm{C}} &= \sum_{n=0}^{\infty} P_n(v_j)\, p_n \\ &\simeq P_0(v_j)\, H + P_1(v_j)\, p_\Sigma(1) \\ &\quad + P_2(v_j)\big(P_{\mathrm{NO}}\, p_{\max}(2) + (1 - P_{\mathrm{NO}})\, p_\Sigma(2)\big) \\ &\quad + \sum_{n=3}^{\infty} P_n(v_j)\, p_\Sigma(n).\end{aligned} \tag{6}$$

The four terms of the summation correspond to the four cases described above. We derive below P_{NO} as well as the probabilities of successful reception of a frame of interest that dominates the sum of interference powers p_Σ, or the maximum power ($p_{\max}$) for a general case of n interfering frames.

P_{NO} of having 2 non-overlapping frames during $2\,\tau_j$ is determined by the probability that the two random transmissions lasting τ_j *do not overlap* over the interval of $2\,\tau_j$. Two transmissions A and B do not overlap, if either A starts in the first half of the $2\,\tau_j$ interval and B comes after A is complete, or vice versa:

$$\begin{aligned}P_{\mathrm{NO}} &= \frac{1}{4\tau_j^2}\int_0^{\tau_j}\int_{\tau_j+x}^{2\tau_j} dy\, dx + \frac{1}{4\tau_j^2}\int_{\tau_j}^{2\tau_j}\int_0^{x-\tau_j} dy\, dx \\ &= \frac{1}{4}.\end{aligned} \tag{7}$$

So, 3/4 of frames with two overlapping transmissions face the sum of their powers, whereas 1/4 of frames have to overcome the strongest one.

*1) **Frame Reception Probability** $p_\Sigma(n)$ **in presence of** n **Colliding Transmissions**:* consider a frame of interest transmitted against n other colliding transmissions, on top of baseline constant interference and noise. For a frame to be successfully received, two conditions need to be satisfied:

1) the fast fading channel gain for this transmission is above g_j, so that the received power is above sensitivity for a given *SF*, and
2) the frame of interest dominates the interference power by factor ξ. The gateway can correctly receive a frame subject to collisions, as long as its power margin ξ is sufficient for successful demodulation. Croce et al. have experimentally determined the value of 1 dB for ξ [40].

Starting from the probability density of the sum of n variables following the $\exp(1)$ distribution: $f_\Sigma(n,x) = \frac{e^{-x}\,x^{n-1}}{(n-1)!}$, we derive $p_\Sigma(n)$, the probability of successful reception of a frame of interest transmitted in presence of n other colliding transmissions. $p_\Sigma(n)$ captures at the same time the impact of thermal noise and the presence of n interfering frames (see derivation in Appendix A) [20]:

$$\begin{aligned}p_\Sigma(n) &= \int_0^{\infty} f_\Sigma(n,x)\int_{\max(g_j,\xi x)}^{\infty} e^{-y}\, dy\, dx \\ &= \frac{1}{(n-1)!}\left(e^{-g_j}\gamma\left(n, \frac{g_j}{\xi}\right)\right. \\ &\quad \left. + \frac{1}{(\xi+1)^n}\Gamma\left(n, \frac{(\xi+1)g_j}{\xi}\right)\right),\end{aligned} \tag{8}$$

where $\gamma(n,x)$ is the lower incomplete gamma function and $\Gamma(n,x)$ is the upper incomplete gamma function.

*2) **Frame Reception Probability** $p_{\max}(n)$ **against** n **Non-overlapping Transmissions**:* the density function of the maximum of n random variables is $f_{\max(X_1 \ldots X_n)}(x) = n[F_X(x)]^{n-1} f_X(x)$, where F_X is the distribution function of X and f_X the density. For n variables distributed according to $\exp(1)$, $f_{\max}(n) = n(1-e^{-x})^{n-1}e^{-x}$.

In the case of $n = 2$ transmissions that do not overlap each other, the probability of dominating the maximum power as well as thermal noise is thus (see derivation of $p_{\max}(n)$ in Appendix B):

$$\begin{aligned}p_{\max}(2) &= \int_0^{\infty} f_{\max}(2)\int_{\max(g_j,\xi x)}^{\infty} e^{-y}\, dy\, dx \\ &= e^{-g_j}\left(1 - e^{-\frac{g_j}{\xi}}\right)^2 + 2\sum_{k=0}^{1}\frac{e^{-g_j\frac{k+\xi+1}{\xi}}}{k+\xi+1}.\end{aligned} \tag{9}$$

E. PDR with Capture and Receiver Diversity

We consider a simple case of diversity with two gateways at a short distance of each other although far enough to reshuffle the fast fading random gain. For instance, this setup may represent a gateway with two cross-polarized antennas.

With receiver diversity, reception is successful unless interference and (or) noise drown out the signal on both antennas. In other words, for each case listed in Section III-D, if the probability of success without diversity is p_c, then with diversity, it is:

$$p_c' = (1 - (1 - p_c)^2) \tag{10}$$

and we need to replace H, $p_\Sigma(1)$, $p_\Sigma(2)$, $p_{\max}(2)$, $p_\Sigma(n)$ in Eq. 6 with the corresponding values computed according to Eq. 10. Thus, the reception probability with diversity becomes:

$$\begin{aligned}\boldsymbol{P}_{\mathrm{C+D}} &\simeq P_0(v_j)\,\left(1 - (1-H)^2\right) + P_1(v_j)\,\left(1 - (1 - p_\Sigma(1))^2\right) \\ &\quad + P_2(v_j)\left(\frac{3}{4}\left(1 - (1 - p_\Sigma(2))^2\right) + \frac{1}{4}\left(1 - (1 - p_{\max}(2))^2\right)\right) \\ &\quad + \sum_{n=3}^{\infty} P_n(v_j)\,\left(1 - (1 - p_\Sigma(n))^2\right).\end{aligned} \tag{11}$$

Notice that, in this model, for each antenna, the probability of dominating thermal noise is not independent of overcoming interfering frames. So, successful frame reception involves verifying both conditions on at least one of the two antennas, which is more realistic than assuming the case of dominating thermal noise on one antenna and interference on the other as considered by Hoeller et al. [26].

IV. Model Results and Comparison with Simulations

In this section, we use the model and simulations to study the *PDR* and the utilization in LoRaWAN, and compare them with the traditional ALOHA model for the cases with and without receiver diversity.

This article has been accepted for publication in IEEE Internet of Things Journal. This is the author's version which has not been fully edited and content may change prior to final publication. Citation information: DOI 10.1109/JIOT.2023.3280393

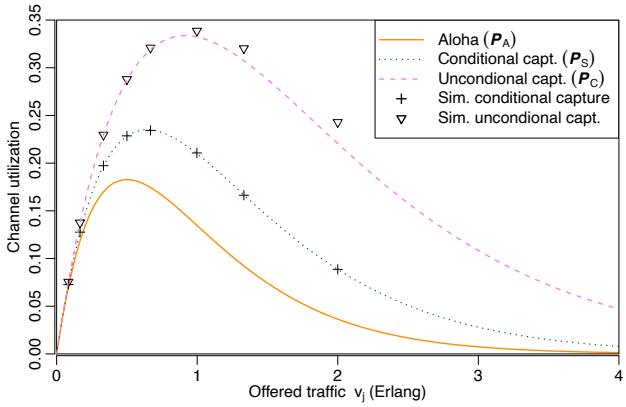

Figure 2. Channel utilization as a function of load for three *PDR* models with all nodes at 2.5 km from the gateway and comparison with simulation. For $\boldsymbol{P}_{\mathrm{C}}$, reception is subject to dominating the sum of interference by factor ξ = 1 dB. For high load, the approximation of overlapping frames for $n > 2$ causes the model to underestimate *PDR*, compared to the result obtained by simulation (▽). Compared to ALOHA ($\boldsymbol{P}_{\mathrm{A}}$) or reception subject to finding an empty channel ($\boldsymbol{P}_{\mathrm{S}}$, simulations: +) [20], maximal utilization is much higher and for a higher load.

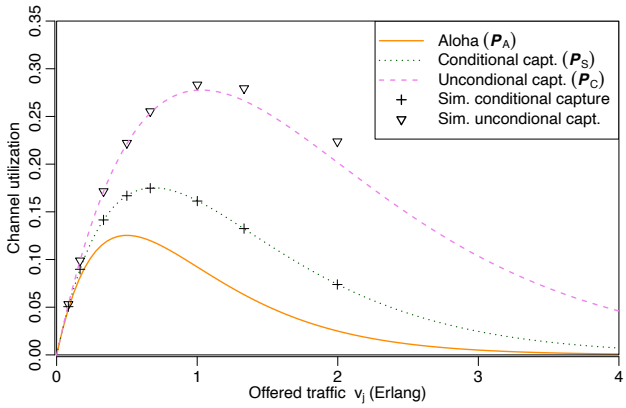

Figure 3. Channel utilization as a function of load for three *PDR* models with all nodes at 7.5 km from the gateway, and comparison with simulation results (+ and ▽). For $\boldsymbol{P}_{\mathrm{C}}$, reception is subject to dominating the sum of interference by factor ξ = 1 dB. The model slightly underestimates *PDR* when the load is high, beyond maximal channel utilization.

A. Traditional ALOHA Model

For comparisons, we recall the traditional unslotted ALOHA model in which any transmission overlapping with another one is considered as lost. *PDR* of unslotted ALOHA is as follows:

$$\boldsymbol{P}_{\mathrm{A}} = H\, e^{-2\,v_j}, \tag{12}$$

because a frame may be lost whenever its transmission overlaps a preceding or a succeeding frame, regardless of the reception power of the interference (H is given by Eq. 1).

With diversity, the probability of successful packet delivery is:

$$\boldsymbol{P}_{\mathrm{A+D}}(v_j) = \left(1 - (1-H)^2\right)\, P_0(v_j), \tag{13}$$

as there are as many random draws for the fast fading gain as receiving antennas.

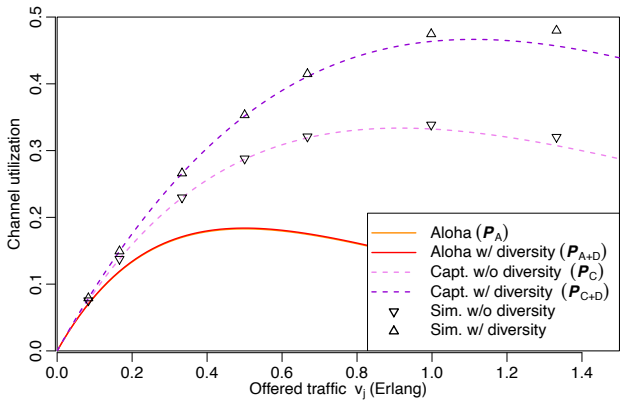

Figure 4. Channel utilization as a function of load for *PDR* models compared with simulation results. For $\boldsymbol{P}_{\mathrm{C}}$, reception is subject to dominating the sum of interference by factor ξ = 1 dB, all nodes are at 2.5 km from the gateway, with and without diversity.

B. PDR for LoRaWAN

Figures 2 and 3 present channel utilization as a function of load for three *PDR* models: i) unslotted ALOHA, ii) reception conditioned by a free channel upon frame arrival ($\boldsymbol{P}_{\mathrm{S}}$), and iii) without this condition—the result of the present model ($\boldsymbol{P}_{\mathrm{C}}$). $\boldsymbol{P}_{\mathrm{S}}$ in the figure is the probability of successful transmission when frame reception is conditioned by a free channel when reception starts. The results of the present $\boldsymbol{P}_{\mathrm{C}}$ model match our earlier NS3 simulations [20] for which the capture assumptions are different. In those simulations, we assumed that an earlier frame would prevail against a later transmission if it came with only 0 dB margin, whereas 6 dB or 8 dB margin would be necessary for a later frame to prevail. The simulation used 6 dB or 8 dB depending on whether the preambles were overlapping or disjoint.

The ability of the SX1302 chip to still receive a stronger frame when a reception is ongoing ($\boldsymbol{P}_{\mathrm{C}}$), makes the capacity increase very significantly compared to $\boldsymbol{P}_{\mathrm{S}}$. The load for maximal utilization also increases to around 1 Erlang. At 2.5 km, maximal channel utilization goes from 24% to 33%, for channel load of 0.64 Erlang and 0.91 Erlang, respectively.

We compare the present model ($\boldsymbol{P}_{\mathrm{C}}$) with simulation results obtained with a LoRaWAN discrete event simulator written in Python[4]. The simulator focuses on a single LoRa frequency channel used by a large number of nodes and takes into account Rayleigh fading, capture, as well as co-SF and inter-SF interference [12]. It needs only a few minutes to simulate a hundred thousand frame transmissions. The simulation results match well the theoretical models that are themselves in line with the output of the much more complete but slower NS-3 simulator used in previous work [20].

For $\boldsymbol{P}_{\mathrm{C}}$, the model and simulation results differ by at most a few percentage points in channel utilization, a small difference related to the approximation adopted above (see Case 4 in Section III-D).

[4]https://gricad-gitlab.univ-grenoble-alpes.fr/heussem/lora-simple-discrete-event-simulator

This article has been accepted for publication in IEEE Internet of Things Journal. This is the author's version which has not been fully edited and content may change prior to final publication. Citation information: DOI 10.1109/JIOT.2023.3280393

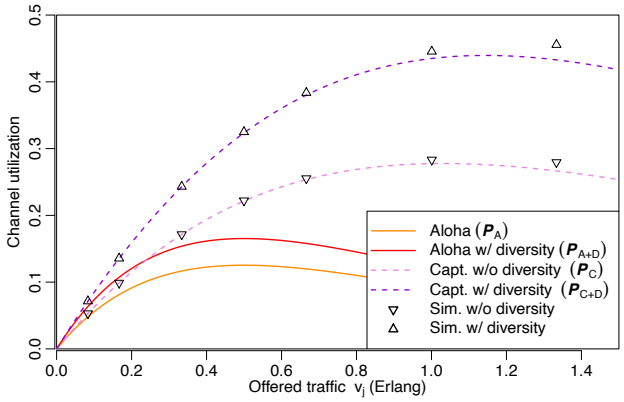

Figure 5. Channel utilization as a function of load for *PDR* models compared with simulation results (▽). All nodes at 7.5 km from the gateway, with and without diversity.

C. Channel Utilization with Diversity

Figures 4 and 5 illustrate the benefits of receiver diversity with maximum utilization substantially increased from 33% to 47% at 2.5 km. Utilization reaches the maximum for a load of more than 1 Erlang, whereas it is 0.91 without diversity.

The next section discusses the implications of the proposed model on using the channel at such high loads and achieving good transmission reliability despite *PDR* of the order of 30-50%.

V. Maximal Utilization and Error Correcting Codes

Utilization essentially represents the proportion of traffic that the channel can handle, relative to its raw capacity. For the values lower than the maximal utilization, the channel can convey more and more data when load increases. Conversely, beyond the maximal utilization, the channel transports less and less data for more load, as transmissions are gradually more detrimental to each other due to collisions.

Packet loss in LoRaWAN remains low if the load is light and at the same time, the mean reception power is well above sensitivity (e.g., see Figure 4 for load significantly less than 1 Erlang). Otherwise, losses from both fast fading and collisions are inevitable and so, reliable data delivery requires the use of some form of inter-packet error correcting code [21], [41], [42], [27]. After recalling below the basics of ECC, this section presents the relationship between maximal channel utilization and the coding rate, the main parameter of ECC.

A. Reliable data delivery with ECC

The general principle of an inter-packet ECC is to transmit data redundantly and, in presence of packet losses, to process the received information to rebuild the missing data. Specifically, systematic codes operate by first transmitting a data packet and then, sending redundant packets that allow reconstruction of the data packet in case of a loss.

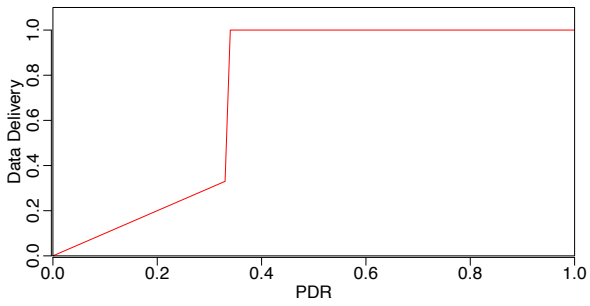

Figure 6. Application Data Delivery Ratio (*DDR*) vs. *PDR* for a perfect systematic error correcting code with coding rate $C = \frac{1}{3}$.

ECC coding rate C defines the level of redundancy above which an inter-packet error correction mechanism becomes effective in case of packet erasures: it has to be at most

$$C = \frac{1}{N_t}, \tag{14}$$

where N_t is the number of transmissions per successful frame reception, the inverse of *PDR*:

$$N_t = \frac{1}{PDR}. \tag{15}$$

This value of C compensates for $N_t - 1$ losses per successful reception. With perfect ECC, if the *PDR* is below C, then error correction is not effective, and the application only gets the data found in the received systematic frames. If $PDR \geq C$, then error correction succeeds and the Data Delivery Rate (*DDR*) goes to 1:

$$\begin{cases} DDR = PDR & \text{if } PDR < C \\ DDR = 1 & \text{otherwise.} \end{cases}$$

Figure 6 shows the *DDR* with respect to the *PDR* for $C = \frac{1}{3}$. A real ECC implementation can be as close to perfect ECC as needed by building redundancy packets from the combination of a larger number of data packets [41], [42].

When analyzing the performance of a network with ECC, it is useful to consider the *goodput*. As we assume that all nodes generate the same traffic load, goodput at data rate DRj is $C \times \lambda_j \times PL_{\max} \times 8$ b/s, as long as the *PDR* is above C. G, the goodput normalized by the channel capacity is thus as follows:

$$\begin{cases} G = C \times v_j & \text{if } PDR > C \\ G = C \times U & \text{otherwise.} \end{cases}$$

When the *PDR* is lower than the ECC coding rate C, the redundancy frames participate to channel contention but they have no beneficial effect on goodput. Conversely, if the *PDR* is above C, the goodput is not optimal either, as some received frames are redundant and not necessary for reliable application data delivery.

B. Maximizing goodput

With the objective to use the LoRa network at its maximum capacity—without excess redundancy nor unacceptable data losses—and based on the models in the previous sections,

This article has been accepted for publication in IEEE Internet of Things Journal. This is the author's version which has not been fully edited and content may change prior to final publication. Citation information: DOI 10.1109/JIOT.2023.3280393

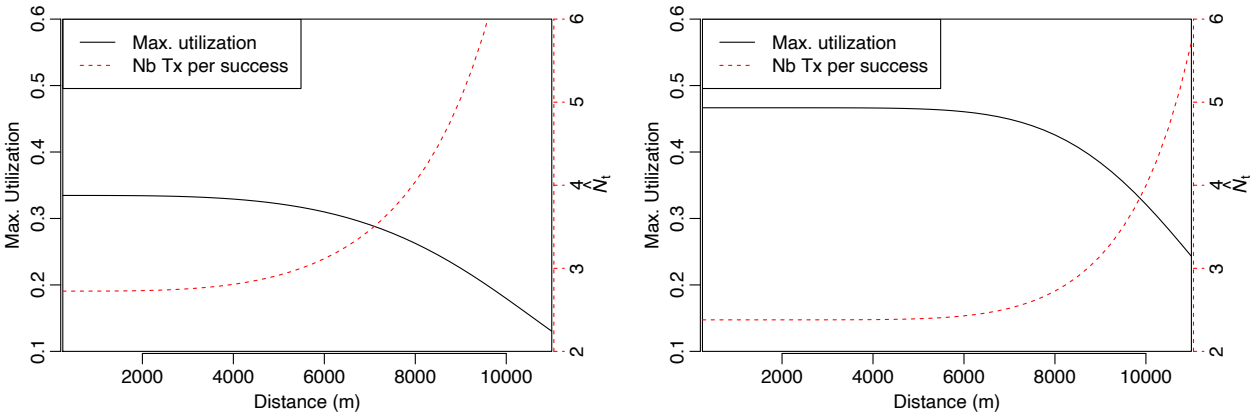

(a) Without diversity (b) With diversity

Figure 7. Maximal utilization $U_{\max}$ (in black) and the number of frame transmissions per successful reception $\hat{N}_t$ (right-hand side scale) vs. distance, *SF12*

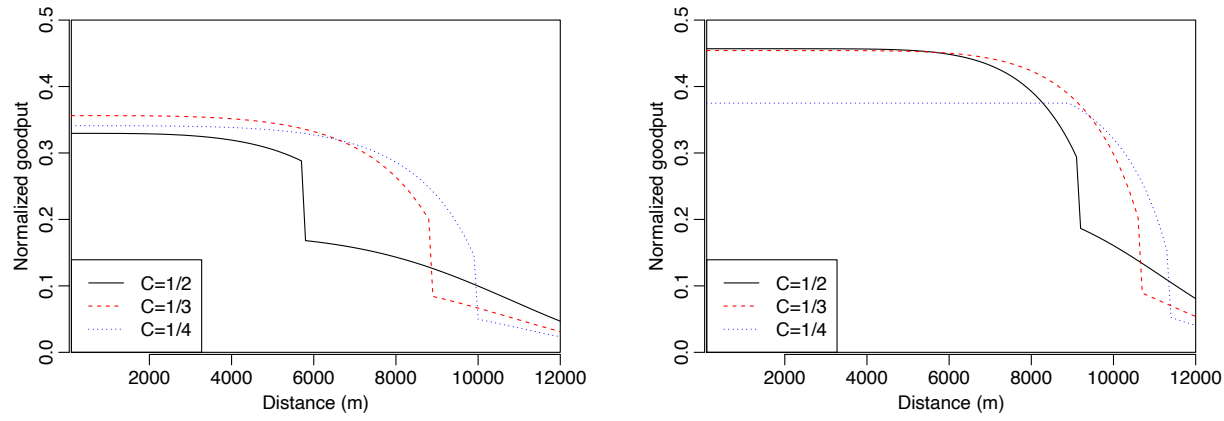

(a) Without diversity (b) With diversity

Figure 8. Best attainable normalized goodput G vs. distance, for perfect ECC with coding rates $C = \frac{1}{2}$, $\frac{1}{3}$, and $\frac{1}{4}$

we have computed the maximal utilization as a function of the distance for the case without and with receiver diversity (see Figure 7). As expected, maximal utilization $U_{\max}(d)$ at distance d has a decreasing trend: at large distances, maximal utilization tends to zero, whereas it is only limited by collisions at a short distance. We can however notice a remarkable fact: **utilization $U_{\max}$ stays almost flat for a wide range of distances**, up to 4 km and up to 6 km, for the case without and with diversity, respectively.

In the figures, we also plot $\hat{N}_t$, the number of transmissions per successful frame reception at maximal utilization:

$$\hat{N}_t = \frac{\hat{v}_j}{U_{\max}} = \frac{1}{PDR_{\max}}, \tag{16}$$

where $\hat{v}_j$ is the load at maximal utilization.

Similarly to $U_{\max}$, $\hat{N}_t$ does not vary much over a wide range of distances, for instance, $\hat{N}_t$ remains below 3 up to a distance of 5.5 km, without diversity, although 15% of frames are lost due to attenuation alone because $H = 0.85$ at this distance for *SF12*. We can notice from Figure 7 that in the disk of 5.5 km, $\hat{N}_t$ stays between 2 and 3 regardless of using diversity. This invariant value of $\hat{N}_t$ is a characteristic of the LoRaWAN cell, which gives us an important result regarding redundancy: **a coding rate of $\frac{1}{3}$ provides an ample margin against losses over a wide range of distances and load**. Typically, $C = \frac{1}{3}$ allows us to resist the loss rate increase up to maximal utilization, with a safety margin. If the ECC is powerful enough to accommodate the loss rate at maximal utilization ($1 - \frac{1}{\hat{N}_t}$), then we can use the network at its maximum. Otherwise, if the ECC coding rate provides insufficient redundancy and/or the ECC is not effective enough, capacity is wasted as the goodput plateaus at a load level lower than the one corresponding to maximal utilization. Conversely, too much redundancy (e.g., $C = \frac{1}{4}$) increases the overhead with little benefits other than better safety margins.

The main takeaway is that if we want to obtain high application data delivery ratio when load is significant, then **the error correction mechanism needs to have the potential to handle the loss rate at maximal utilization**. As we face an erasure channel, the coding rate needs to be low enough to

provide robustness matching the order of magnitude of *PDR*.

Using a coding rate different from the value corresponding to $\hat{N}_\mathrm{t}$ for the considered distance always reduces the goodput. To illustrate this fact, we can compute the number of nodes in a cell for various values of C, assuming that the nodes are all at 6 km, without diversity and assuming perfect error correction for simplicity:

- **Maximal utilization**. The *PDR* is $\frac{1}{3}$ for a load of 0.93 Erlang and, at this point, *utilization is at its maximum* of 31%. Using data rate DR0, this load corresponds to $m_0 = 279$ nodes with 0.33% duty cycle ($m_0 = \frac{v_0}{\tau_0 \lambda_\mathrm{t}}$), which is the maximal number of nodes that may benefit from reliable data delivery under condition that they use a perfect inter-packet ECC with $C = \frac{1}{3}$.
- **Higher coding rate** $C = \frac{1}{2}$. If nodes use a coding rate of $C = \frac{1}{2}$, the *PDR* needs to be at least $\frac{1}{2}$ for reliable delivery, which happens for the load of 0.53 Erlang and utilization of 27%. This load corresponds to $m_0 = 159$ nodes with 0.33% duty cycle. Compared to the case above, utilization is lower and hence, the number of nodes is smaller, which comes as no surprise. However, a more relevant comparison is to consider the number of nodes with the same application traffic as for $C = \frac{1}{3}$, so with 0.22% duty cycle. Then, the number of nodes is $m_0 = 239$, still lower than for $C = \frac{1}{3}$. On the one hand, the traffic load decreases because nodes transmit less redundant packets, which creates less collisions. On the other hand, the smaller *PDR* corresponds to a smaller utilization, which is what limits the number of nodes, somewhat counter-intuitively.
- **Lower coding rate** $C = \frac{1}{4}$. The load of 1.2 Erlang, *higher than for maximum utilization*, gives a PDR of $\frac{1}{4}$. The utilization is 30%, which corresponds to $m_0 = 271$ nodes with the same application traffic load as for $C = \frac{1}{3}$, so 0.44% duty cycle (which would exceed the band duty cycle limitation). In this case, at the point at which the ECC is used at its best with exactly no excess redundant packet transmissions ($C = PDR$), the loss rate is high and the load is greater than $\hat{v}_j$. If nodes generated a smaller load corresponding to maximal utilization $\hat{v}_j$ with $C = \frac{1}{4}$, their traffic would include unnecessary redundant information, so some channel capacity would be wasted. Moreover, the error correction mechanism becomes overly computationally intensive.

In other words, when the channel gain is high and $H \lesssim 1$, then $\hat{N}_\mathrm{t}$ is well below 3 for maximal utilization (e.g., for the distance less than 8 km with diversity and *SF12*), an ECC coding rate smaller than $\frac{1}{3}$ would be counter-productive, as the channel would convey unneeded redundant information ($C = \frac{1}{3}$ is in fact already a safe choice).

Nevertheless, more redundancy (lower C) allows increasing the coverage range and maintaining a reliable data transfer even if H decreases. Moreover, a lower coding rate than $\frac{1}{\hat{N}_\mathrm{t}}$ gives margin to compensate for the ECC mechanism imperfection.Using a lower C also allows data delivery with lower latency by means of using for example a low depth redundancy window, which makes the ECC less effective.

Another notable fact is the insensitivity of $\hat{N}_\mathrm{t}$ for maximal utilization to the value of ξ. The figures appear in Appendix: with $\xi = 3$ dB for instance, utilization significantly drops compared to the case of $\xi = 1$ dB (i.e., with a plateau at less than 40% with diversity) but $\hat{N}_\mathrm{t}$ remains well below 3.

C. Choice of the ECC Coding Rate

Figure 8 shows G, the best attainable normalized goodput for various coding rates. Each point of the curves comes from finding the load of maximal goodput at each distance. For all values of C, G stays at first mostly flat when the distance increases, before the required redundancy starts to grow in face of channel losses, so nodes need to switch to more robust ECC (lower C). In Figure 8(b), $C = \frac{1}{2}$ and $C = \frac{1}{3}$ give similar results but the latter has a margin for ECC imperfection, whereas the former is too weak to reach best utilization and ECC imperfection would further degrade goodput.

VI. SF Allocation and Cell Capacity

As the previous section concludes that coding rate $C = \frac{1}{3}$ is needed to compensate for losses at maximal utilization unless we seek to extend coverage, it seems natural to use this value as the starting point to optimize the transmission parameters within a cell.

We recall our assumption that the packet generation process of all nodes is the same, and it represents the traffic intensity that would match the duty cycle limitation for *SF12* transmissions (applications do not generate more traffic when changing to a lower *SF*). In case of inter-packet ECC, the generation intensity of application layer data needs to be lower (by a factor C) to make room for redundancy, or alternatively, the nodes could refrain from using higher *SFs*, and then, capacity in terms of the number of nodes would need to be scaled down. We do not limit the cell radius to a specific value, so the *SF12* zone is effectively infinite and we focus only on the results with *SF7* to *SF11*.

A. SF Allocation

Using the analysis in the previous sections, we can find by dichotomy where the *SF7* to *SF8* boundary needs to be placed to get a target *PDR* of a given value, if we had perfect power control and all nodes were virtually placed at this limit. The target *PDR* value of 0.4 seems to be the right choice for the case of using ECC—the target *PDR* slightly above 0.33 gives a safety margin for recovering from transmissions losses with the inter-packet ECC coding rate of $\frac{1}{3}$. When the *SF* boundary moves farther away from the gateway, more nodes can use *SF7* so there are more collisions but at the same time, the nodes at the outer edge of the zone suffer from more and more losses due to path loss. Once the first limit is found for the *SF7*/*SF8* boundary, we repeat the same procedure for the next *SF* zone limit, etc.

Figures 9 and 10 illustrate this *SF* allocation for the node densities of 20 and 90 nodes per square km.We can observe that for small *SFs* and low node density in Figure 9, the radio channel is lightly loaded. In this area, the *PDR* is constrained

This article has been accepted for publication in IEEE Internet of Things Journal. This is the author's version which has not been fully edited and content may change prior to final publication. Citation information: DOI 10.1109/JIOT.2023.3280393

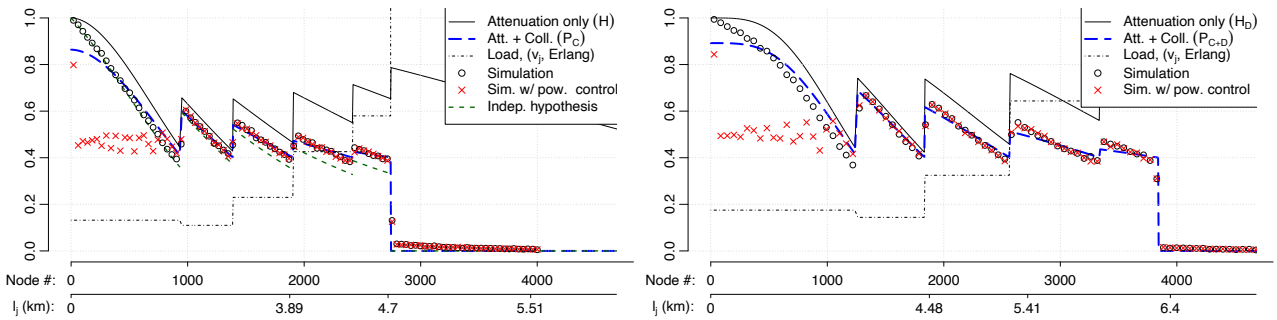

(a) Without diversity (b) With diversity

Figure 9. Packet delivery ratio with the *SF* allocation targeting *PDR* of at least 0.4, medium node density of 20 nodes per km^2. ○: simulation without power control, ×: simulation with power control in the *SF7* zone. The cell covers the range of 6.6 km for *SF7* – *SF11* with 2746 nodes, and 7.8 km with 3844 nodes, without and with diversity, respectively. The 'independence hypothesis" curve is the model by de Souza Sant'Ana et al. [27], [13] discussed in Subsection VI-C.

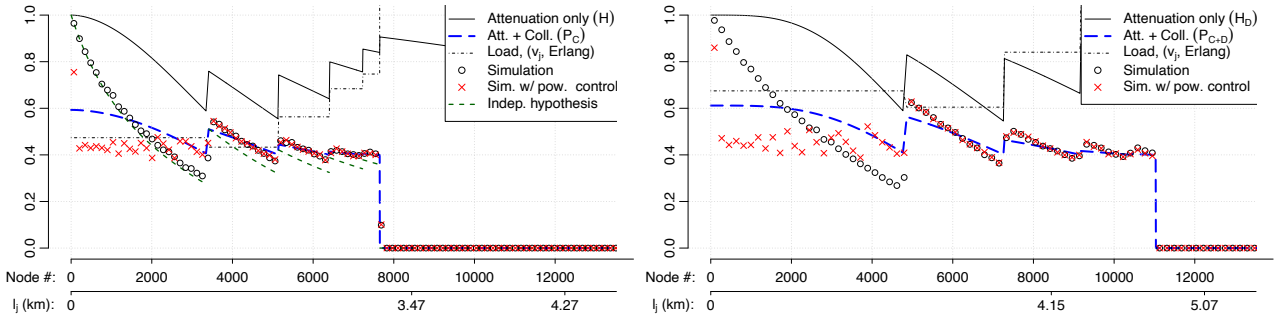

(a) Without diversity (b) With diversity

Figure 10. Packet delivery ratio with the *SF* allocation targeting *PDR* of at least 0.4, high node density of 90 nodes per km^2. ○: simulation without power control, ×: simulation with power control in the *SF7* zone. The cell covers the range of 5.2 km for *SF7* – *SF11* with 7654 nodes, and 6.2 km with 11036 nodes, without and with diversity, respectively. The 'independence hypothesis" curve is the model by de Souza Sant'Ana et al. [27], [13] discussed in Subsection VI-C.

by the radio range. For larger *SFs*, the load and utilization increase and the channel becomes contention-constrained. When node density is higher (see Figure 10), especially with diversity, the load is more evenly spread between *SFs* and utilization is closer to the optimum.

B. What Simulation Tells Us

We have run simulations with the *SF* boundaries found by dichotomy. Complementing the theoretical model, the simulation takes into account the fact that nodes in a given *SF* zone actually face dissimilar average path loss to the gateway(s) as they are not all located at the edge of the *SF* zone. Moreover, the same nodes will face contention when their packets collide with the ones sent by closer nodes. This problem is the most prominent in the *SF7* zone without power control, as it is a disc where we find more contrasted path loss values compared to the more homogeneous ones in the other zone annuli. The simulation statistics are computed for 1 million packet transmissions and homogeneous density of sources (confidence intervals are not shown as they are of the order of 1 percentage point).

In Figure 9, the *PDR* obtained by simulation (without power control) closely matches the theoretical values, even though the analysis is based on a model in which the nodes are all virtually placed at the outer edge of the considered *SF* annulus. The nodes in the outer part of each *SF* zone face a slight disadvantage but the impact is limited, due to a low level of contention.

In contrast, in Figure 10, compared to the analysis, the *PDR* obtained by simulation is noticeably lower for the nodes located in the outer part of the SF annuli, although, again, the analysis considers that all nodes are at the *SF* zone edge. While it may be surprising at first that having some nodes closer to the gateway yields worse results, what happens is that, as soon as a fraction of the nodes benefit from a better channel, the probability of capture drops for the more remote senders.

With high node density, the combination of having capture capability and a low target *PDR* allows operating the network at a high load level: sometimes more than 1 Erlang, whereas it would be limited to about 0.2 Erlang with more conservative assumptions [12]. The high load, in turn, increases the probability of collision so, there is a greater impact on the *PDR*

This article has been accepted for publication in IEEE Internet of Things Journal. This is the author's version which has not been fully edited and content may change prior to final publication. Citation information: DOI 10.1109/JIOT.2023.3280393

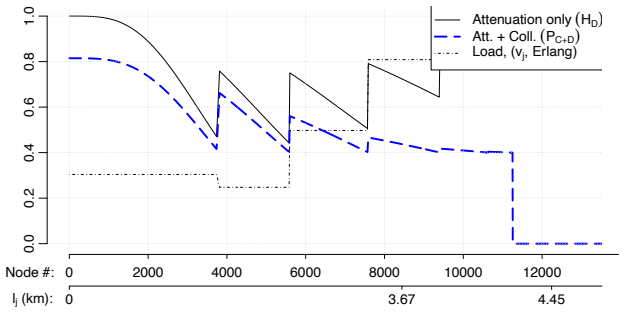

Figure 11. Adding *SF6*, for high node density and with diversity; the capacity gain is limited

experienced by the nodes in the outer part of each *SF* zone, in particular for the nodes using *SF7*.

C. Comparison with Previous Work: H and Q_1 as Independent Probabilities

In Figures 9(a) and 10(a), we plot the *PDR* computed according to the model by de Souza Sant'Ana et al. [27], [13]. They assume that overcoming noise with probability H is independent of Q_1, the probability of dominating the sum of interference. The model fits quite well the *PDR* obtained throughout the *SF7* zone, as the model of Q_1 accounts for near-far effects in collisions, which $\boldsymbol{P}_S$ does not capture. So, the product HQ_1, which assumes independence between the factors, conforms better to the simulation than $\boldsymbol{P}_S$ for the nodes located near the gateway. Nevertheless, for larger *SFs*, and to a lesser extent in the outer part of the *SF7* zone, the independence assumption leads to significantly under-evaluating the *PDR*. Within each of these zones, there is a little contrast between the channel gains of the nodes so the collisions are less asymmetric (i.e., asymmetric collisions: between frames of widely differing powers) than near the gateway, and the precision of Q_1 is less relevant: the dominant factor for the *PDR* variations within each zone other than SF7 is rather the evolution of H.

The next section discusses power control in the SF7 zone: among other benefits, power control makes the channel more uniform and collisions more symmetric (and thus makes the precision of Q_1 less relevant).

D. Power Control in the SF7 Zone

In Figures 9 and 10, we also plot the PDR obtained by simulation with power control in the *SF7* zone. For high node density in Figure 10 and without power control, asymmetrical collisions are very detrimental for a large number of nodes using *SF7*, regardless of the availability of receiver diversity.

Power control is obviously a good means to lessen the impact of large channel gain differences. In the LoRaWAN standard, power control has a 12 dB scale, which does not allow to even up the PDR throughout the *SF7* zone. Power control in the figures has a 24 dB range with increments of 2 dB.

Again, it may seem counterintuitive at first that high node density increases the need for power control and calls for a greater adjustement magnitude, as the nodes in the SF7 zone are more grouped together when density is high. Nevertheless, even though the density is more than 4 times more important in Figure 10 compared to Figure 9, the radius of the *SF*7 zone does not change much, whereas the presented load are not of the same order of magnitude. In other words, even though the SF7 discs are of comparable surface (only 12% larger for smaller node density with diversity), the limiting factors are not the same: the PDR falls steeply when approaching the *SF7* radio range for smaller density, whereas collisions are the problem for higher density.

E. Adding SF6

For high node density, it is thus apparent that the *SF7* zone saturates, so that some nodes switch to *SF8* even though they are still within the *SF7* coverage range. We consider the *SF* allocation including *SF6*, not defined in the LoRaWAN specification but supported by Semtech chips (see Figure 11). It turns out that the total number of covered nodes is very similar around 11000, although the load is greatly reduced in the *SF7* zone, as expected. In terms of node capacity, the benefit of adding *SF6* would consist of accommodating higher node density or an inhomogeneous node spatial distribution.

F. Inter-SF Interference

As the channel load is high for all *SFs*, most transmissions not only interfere with other transmissions in the same *SF*, but also with overlapping transmissions using other *SFs*. To assess the impact of inter-SF collisions, we use the power margins experimentally found for a successful reception in presence of inter-SF interference [40]. Figure 12 shows that there is little impact of the farther nodes on those closer to the gateway, even though the latter uses a less robust modulation (*SF7*). On the contrary, the high *SF7* traffic load significantly reduces the *PDR* for farther nodes, despite the fact that LoRa modulations are much less sensitive to interference caused by smaller *SFs* than to that of higher *SFs*.

We can see in Figure 12 that it is sufficient to reduce the transmission power of the nodes experiencing a good channel gain in the *SF7* zone to mostly erase the effect of the inter-SF interference. For SF8 to SF12, the simulation results obtained by taking into account inter-SF interference are in good agreement with both the model and simulations set to ignore this problem (the red stars in Fig. 12 are similar to the red crosses in Fig. 10, near the blue lines).

VII. Conclusion

In this paper, we have proposed a new model of unslotted ALOHA with capture and multiple collisions in LoRaWAN. Unlike other previous LoRaWAN models, we assume that channel conditions are the same for both deciding if a frame can be successfully demodulated and if it dominates the sum of co-SF interference. The model results in an accurate estimation of *PDR* validated with extensive simulations. One limitation

This article has been accepted for publication in IEEE Internet of Things Journal. This is the author's version which has not been fully edited and content may change prior to final publication. Citation information: DOI 10.1109/JIOT.2023.3280393

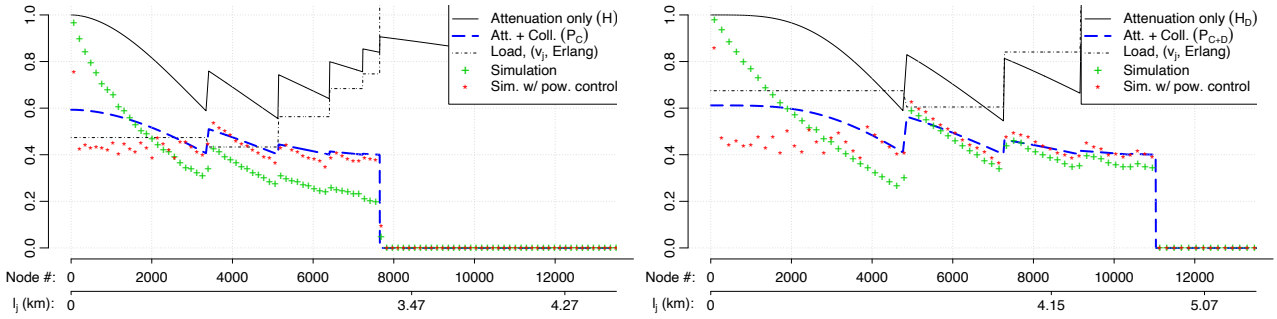

(a) Without diversity (b) With diversity

Figure 12. Packet delivery ratio with inter-SF interference, *SF* allocation targeting *PDR* of at least 0.4, high node density of 90 nodes per km^2. $+$: simulation without power control, $\star$: simulation with power control in the *SF7* zone. Power control is very effective to obviate the impact of imperfect orthogonality.

of the model is that it does not capture inter-SF interference and assumes that all nodes using the same *SF* are at the same distance from the gateway. We thus use simulations to assess the impact of these phenomena and conclude first, that they are notable and second, that using power control in the *SF7* zone only is sufficient to attenuate their effects.

We apply this model to find the required ECC coding rate that coincides with the maximum channel utilization and it emerges that coding rate $C = \frac{1}{3}$ is enough to cover a wide cell range. Notably, when the load is high and the dominant cause of losses are collisions, the same coding rate of $C = \frac{1}{3}$ is the one for which reliable application data delivery is attained while approaching maximal channel utilization. Moreover, we show that a coding rate of $\frac{1}{2}$ does not allow reaching maximal capacity, which confirms previous findings [12], [27], and provides a theoretical framework for these results. We also observe that more redundancy (lower C) increases the coverage range. In brief, long range communication with ALOHA access incurs fast fading and collisions but inter-packet error correction effectively combats the problem. Moreover, the coding rate of the ECC does not need to be adjusted for each situation as the same coding rate of $C = \frac{1}{3}$ suits most cases, unless we seek wider coverage with lower C.

In the model, we also consider receiver diversity, and show that it brings significant benefits for an increased range and cell capacity. The required ECC coding rate for reliable delivery at maximal utilization is similar to the case of the cell without diversity, unless we want to increase the communication range at a given *SF*. The fact that the coding rate does not change with or without diversity is encouraging for using redundancy in a macro-diversity setup, which is the general case for LoRaWAN networks.

In this work, we have assumed that all nodes use the same coding rate and error correction mechanisms. Since we consider a traffic load that attains the duty cycle limit only for *SF12*, there is room for using lower coding rates at lower *SFs*. Actually, in Figures 9 and 10, the channel load is lighter for low *SFs*: when the node density is low, few nodes occupy low SFs zones and traffic is scarce. A lower coding rate would allow aiming at an even lower *PDR* near the gateway, increasing the radius of the SF boundary, to cover more nodes that would have to transmit with increased redundancy. This in turn enables offloading higher *SFs* and thus, increases coverage. It may appear counterintuitive at first that aiming at a lower *PDR*, which increases the load and losses near the gateway, would extend cell coverage but, just like for the necessity of power control in this area, carefully managing the nodes benefitting from the best communication conditions makes it possible to optimize the cell as a whole.

Appendix A
Probability of Successful Reception in Presence of n Overlapping Frames

The probability of successful reception of a Frame of interest transmitted in presence of n other overlapping transmissions is the probability p_Σ that the Frame of interest dominates both the thermal noise and the interference:

$$
\begin{aligned}
p_\Sigma(n) &= \int_0^\infty f_\Sigma(n,x) \int_{\max(g_j,\xi x)}^\infty e^{-y}\, dy\, dx \\
&= \int_0^{\frac{g_j}{\xi}} f_\Sigma(n,x) \int_{g_j}^\infty e^{-y}\, dy\, dx \\
&\quad + \int_{\frac{g_j}{\xi}}^\infty f_\Sigma(n,x) \int_{\xi x}^\infty e^{-y}\, dy\, dx \\
&= \frac{1}{(n-1)!} \left(e^{-g_j} \int_0^{\frac{g_j}{\xi}} e^{-x} x^{n-1}\, dx \right. \\
&\quad \left. + \int_{\frac{g_j}{\xi}}^\infty x^{n-1} e^{-(\xi+1)x}\, dx \right) \\
&= \frac{1}{(n-1)!} \left(e^{-g_j} \gamma(n, \frac{g_j}{\xi}) \right. \\
&\quad \left. + \frac{1}{(\xi+1)^{n-1}} \int_{\frac{g_j}{\xi}}^\infty \left[(\xi+1)x\right]^{n-1} e^{-(\xi+1)x} dx \right)
\end{aligned}
$$

$$
\begin{aligned}
p_{\Sigma}(n) =& \frac{1}{(n-1)!}\left(e^{-g_j}\gamma(n,\frac{g_j}{\xi}) \right.\\
&\left. + \frac{1}{(\xi+1)^n}\int_{\frac{(\xi+1)g_j}{\xi}}^{\infty} u^{n-1}e^{-u}\,du\right)\\
=& \frac{1}{(n-1)!}\left(e^{-g_j}\gamma\left(n,\frac{g_j}{\xi}\right)\right.\\
&\left. + \frac{1}{(\xi+1)^n}\Gamma\left(n,\frac{(\xi+1)g_j}{\xi}\right)\right),
\end{aligned}
$$

where $\gamma(n,x)$ is the lower incomplete gamma function and $\Gamma(n,x)$ is the upper incomplete gamma function.

Appendix B
Probability of Successful Reception in Presence of n Non-Overlapping Frames

When the concurrent transmissions are non-overlapping, the probability of capture is the likelihood of dominating the thermal noise and the one concurrent transmission with the maximum power.

$$
\begin{aligned}
p_{\max}(n) =& \int_0^{\infty} f_{\max}(n)\int_{\max(g_j,\xi x)}^{\infty} e^{-y}\,dy\,dx\\
=& \int_0^{\frac{g_j}{\xi}} n(1-e^{-x})^{n-1}e^{-x}\int_{g_j}^{\infty} e^{-y}\,dy\,dx\\
&+ \int_{\frac{g_j}{\xi}}^{\infty} n(1-e^{-x})^{n-1}e^{-x}\int_{\xi x}^{\infty} e^{-y}\,dy\,dx\\
=& e^{-g_j}\int_{\frac{g_j}{\xi}}^{\infty} n(1-e^{-x})^{n-1}e^{-x}\,dx\\
&+ \int_{\frac{g_j}{\xi}}^{\infty} n(1-e^{-x})^{n-1}e^{-(\xi+1)x}\,dx\\
=& e^{-g_j}\left(1-e^{-\frac{g_j}{\xi}}\right)^n\\
&+ \int_{\frac{g_j}{\xi}}^{\infty} n\sum_{k=0}^{n-1}\binom{n-1}{k}(-1)^k e^{-(k+\xi+1)x}\,dx\\
=& e^{-g_j}\left(1-e^{-\frac{g_j}{\xi}}\right)^n\\
&+ n\sum_{k=0}^{n-1}\binom{n-1}{k}(-1)^k\frac{e^{-g_j\frac{k+\xi+1}{\xi}}}{k+\xi+1}.
\end{aligned}
$$

Appendix C
Number of transmissions per successful reception at maximum utilization

With $\xi = 3\,\text{dB}$, the results with and without diversity appear in Figure 13.

References

[1] LoRa™ Alliance, "A Technical Overview of LoRa and LoRaWAN," 2015.

[2] N. Sornin, Editor, "LoRaWAN Specification v1.1," 2017. [Online]. Available: https://lora-alliance.org/resource-hub/lorawantm-specification-v11

[3] N. Abramson, "THE ALOHA SYSTEM: Another Alternative for Computer Communications," in *Proceedings of the Fall Joint Computer Conference*, New York, NY, USA, 1970, pp. 281–285.

[4] L. G. Roberts, "ALOHA Packet System with and without Slots and Capture," *SIGCOMM Comput. Commun. Rev.*, vol. 5, no. 2, pp. 28–42, Apr. 1975.

[5] "The Things Network LoRaWAN Limitations." [Online]. Available: https://www.thethingsnetwork.org/docs/lorawan/limitations/

[6] D. Magrin, M. Capuzzo, and A. Zanella, "A thorough study of lorawan performance under different parameter settings," *IEEE Internet of Things Journal*, vol. 7, no. 1, pp. 116–127, 2020.

[7] O. Georgiou and U. Raza, "Low Power Wide Area Network Analysis: Can LoRa Scale?" *IEEE Wireless Communications Letters*, vol. 6, no. 2, Apr. 2017.

[8] Z. Li, S. Zozor, J.-M. Brossier, N. Varsier, and Q. Lampin, "2D Time-Frequency Interference Modelling Using Stochastic Geometry for Performance Evaluation in Low-Power Wide-Area Networks," in *2017 IEEE ICC*, May 2017.

[9] A. Waret, M. Kaneko, A. Guitton, and N. El Rachkidy, "LoRa Throughput Analysis with Imperfect Spreading Factor Orthogonality," *IEEE Wireless Communications Letters*, 2018.

[10] K. Mikhaylov, J. Petäjäjärvi, and T. Hänninen, "Analysis of Capacity and Scalability of the LoRa Low Power Wide Area Network Technology," in *22th European Wireless Conference*, May 2016.

[11] A. Mahmood, E. Sisinni, L. Guntupalli, R. Rondon, S. A. Hassan, and M. Gidlund, "Scalability Analysis of a LoRa Network under Imperfect Orthogonality," *IEEE Transactions on Industrial Informatics*, 2018.

[12] M. Heusse, T. Attia, C. Caillouet, F. Rousseau, and A. Duda, "Capacity of a LoRaWAN Cell," in *MSWiM 2020 - 23rd International ACM Conference on Modeling, Analysis and Simulation of Wireless and Mobile Systems*. Alicante, Spain: ACM, Nov. 2020, pp. 131–140.

[13] J. M. de Souza Sant'Ana, A. Hoeller, R. D. Souza, H. Alves, and S. Montejo-Sánchez, "LoRa Performance Analysis with Superposed Signal Decoding," *IEEE Wireless Communications Letters*, vol. 9, no. 11, pp. 1865–1868, 2020.

[14] C. Goursaud and J.-M. Gorce, "Dedicated Networks for IoT: PHY/MAC State of the Art and Challenges," *EAI Endorsed Transactions on Internet of Things*, vol. 1, no. 1, 10 2015.

[15] D. Magrin, M. Centenaro, and L. Vangelista, "Performance Evaluation of LoRa Networks in a Smart City Scenario," in *IEEE International Conference on Communications (ICC)*, May 2017.

[16] L. Kleinrock and F. Tobagi, "Packet Switching in Radio Channels: Part I - Carrier Sense Multiple-Access Modes and Their Throughput-Delay Characteristics," *IEEE Trans. on Comm.*, vol. 23, no. 12, 1975.

[17] C. Lau and C. Leung, "Capture Models for Mobile Packet Radio Networks," *IEEE Trans. Commun.*, vol. 40, pp. 917–925, 1992.

[18] A. Kochut, A. Vasan, A. U. Shankar, and A. K. Agrawala, "Sniffing Out the Correct Physical Layer Capture Model in 802.11b," in *IEEE ICNP*, Berlin, Germany, 2004, pp. 252–261.

[19] K. Whitehouse, A. Woo, F. Jiang, J. Polastre, and D. Culler, "Exploiting the Capture Effect for Collision Detection and Recovery," in *Proc. the 2nd IEEE Workshop on Embedded Networked Sensors*, 2005, p. 45–52.

[20] T. Attia, M. Heusse, and A. Duda, "Message in Message for Improved LoRaWAN Capacity," in *IEEE International Conference on Computer Communications and Networks (ICCCN)*, Athens, Greece, Jul. 2021.

[21] U. Coutaud, M. Heusse, and B. Tourancheau, "High Reliability in LoRaWAN," in *Proceedings of IEEE PIMRC*, London (virtual conference), United Kingdom, Aug. 2020.

[22] SIGFOX, "Sigfox Technology Overview," 2018. [Online]. Available: {https://www.sigfox.com}

[23] Mioty, "Mioty Alliance," 2022. [Online]. Available: {https://mioty-alliance.com/miotytechnology/}

[24] G. Kilian, M. Breiling, H. H. Petkov, H. Lieske, F. Beer, J. Robert, and A. Heuberger, "Increasing transmission reliability for telemetry systems using telegram splitting," *IEEE Transactions on Communications*, vol. 63, no. 3, pp. 949–961, 2015.

[25] Y. Birk and Y. Keren, "Judicious Use of Redundant Transmissions in Multichannel ALOHA Networks with Deadlines," *IEEE Journal on Selected Areas in Communications*, vol. 17, no. 2, pp. 257–269, 1999.

[26] A. Hoeller, R. D. Souza, O. L. A. López, H. Alves, M. de Noronha Neto, and G. Brante, "Analysis and Performance Optimization of LoRa Networks With Time and Antenna Diversity," *IEEE Access*, vol. 6, pp. 32 820–32 829, 2018.

[27] J. M. de Souza Sant'Ana, A. Hoeller, R. D. Souza, S. Montejo-Sánchez, H. Alves, and M. d. Noronha-Neto, "Hybrid Coded Replication in LoRa Networks," *IEEE Transactions on Industrial Informatics*, vol. 16, no. 8, pp. 5577–5585, 2020.

[28] Q. Song, X. Lagrange, and L. Nuaymi, "Evaluation of Macro Diversity Gain in Long Range ALOHA Networks," *IEEE Comm. Letters*, vol. 21, no. 11, pp. 2472–2475, 2017.

[29] D. Magrin, M. Capuzzo, A. Zanella, L. Vangelista, and M. Zorzi, "Performance analysis of lorawan in industrial scenarios," *IEEE Transactions on Industrial Informatics*, vol. 17, no. 9, pp. 6241–6250, 2021.

This article has been accepted for publication in IEEE Internet of Things Journal. This is the author's version which has not been fully edited and content may change prior to final publication. Citation information: DOI 10.1109/JIOT.2023.3280393

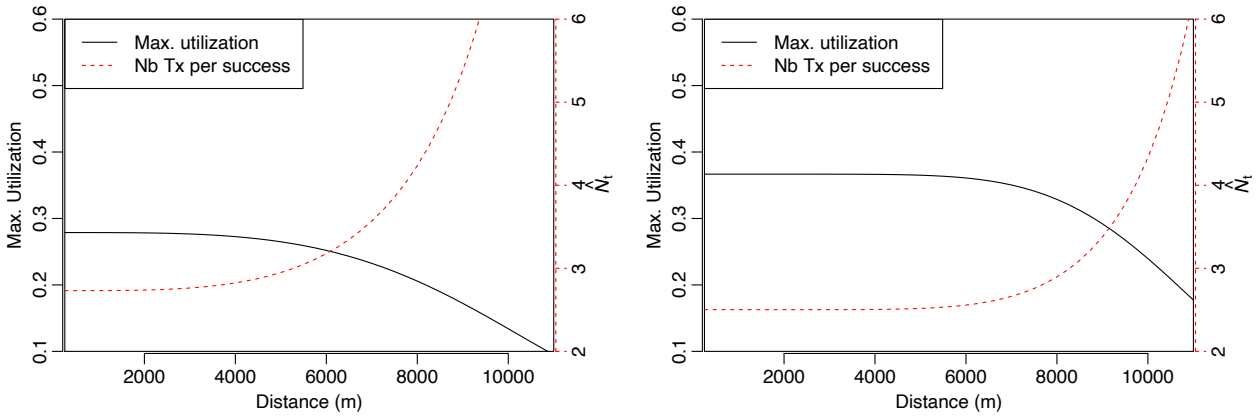

(a) Without diversity

(b) With diversity

Figure 13. Maximal utilization $U_{\max}$ (in black) and number of frame transmissions per successful reception $\hat{N}_t$ (right-hand side scale) vs. distance, *SF12*, $\xi = 3$dB

[30] E. Balevi, F. T. A. Rabee, and R. D. Gitlin, "ALOHA-NOMA for Massive Machine-to-Machine IoT Communication," in *Proc. IEEE ICC, May 20-24,, Kansas City, MO, USA*, 2018, pp. 1–5.

[31] N. Hou, X. Xia, and Y. Zheng, "Don't miss weak packets: Boosting lora reception with antenna diversities," in *IEEE INFOCOM 2022 - IEEE Conference on Computer Communications*, 2022, pp. 530–539.

[32] Z. Wang, L. Kong, K. Xu, L. He, K. Wu, and G. Chen, "Online concurrent transmissions at lora gateway," in *IEEE INFOCOM 2020 - IEEE Conference on Computer Communications*, 2020, pp. 2331–2340.

[33] Q. Chen and J. Wang, "Aligntrack: Push the limit of lora collision decoding," in *2021 IEEE 29th International Conference on Network Protocols (ICNP)*, 2021, pp. 1–11.

[34] Semtech, "SX1272/73 - 860 MHz to 1020 MHz Low Power Long Range Transceiver," 2017.

[35] "LoRaTools Airtime Calculator." [Online]. Available: https://loratools.nl/#/airtime

[36] O. Sellers, "Predicting LoRaWAN capacity," Semtech, Tech. Rep., May 2020.

[37] X. Le, B. Vrigneau, M. Gautier, M. Mabon, and O. Berder, "Energy/Reliability Trade-off of LoRa Communications over Fading Channels," in *IEEE ICT 2018, Saint Malo, France*, 2018.

[38] Wireless & Sensing Products Division, "SX1302 Datasheet Rev 1.2," Semtech, Oct 2020.

[39] A. Rahmadhani and F. Kuipers, "When LoRaWAN Frames Collide," in *12th International Workshop on Wireless Network Testbeds, Experimental Evaluation & Characterization*, ser. WiNTECH '18. ACM, 2018.

[40] D. Croce, M. Gucciardo, S. Mangione, G. Santaromita, and I. Tinnirello, "LoRa Technology Demystified: From Link Behavior to Cell-Level Performance," *IEEE Transactions on Wireless Communications*, vol. 19, no. 2, pp. 822–834, 2020.

[41] U. Coutaud, M. Heusse, and B. Tourancheau, "Fragmentation and Forward Error Correction for LoRaWAN Small MTU Networks," in *MaDe-LoRa workshop, Embedded Wireless Systems and Networks (EWSN)*. ACM, 2020.

[42] P. Marcelis, N. Kouvelas, V. S. Rao, and V. Prasad, "DaRe: Data Recovery through Application Layer Coding for LoRaWAN," *IEEE Transactions on Mobile Computing*, 2020.